1995MNRAS.273..837M

Mon. Not. R. Astron. Soc. **273**, 837–848 (1995)

Angle-dependent Compton reflection of X-rays and gamma-rays

Paweł Magdziarz[1] and Andrzej A. Zdziarski[2]
[1]*Astronomical Observatory, Jagiellonian University, Orla 171, 30-244 Cracow, Poland, Internet: pavel@oa.uj.edu.pl*
[2]*Copernicus Astronomical Center, Bartycka 18, 00-716 Warsaw, Poland, Internet: aaz@camk.edu.pl*

Accepted 1994 November 24. Received 1994 November 4

Downloaded from https://academic.oup.com/mnras/article/273/3/837/1056423 by guest on 20 August 2022

ABSTRACT

Using a Monte Carlo method, we derive approximations to Green's functions for the Compton reflection of X-rays and γ-rays by cold electrons. In Compton reflection, X-rays and γ-rays emitted by a source impinge upon a slab (e.g., an accretion disc) and re-emerge with a spectrum altered by Compton scattering and bound-free absorption. The obtained Green's functions are dependent on the viewing angle of the reflecting slab, which extends the previous treatments of the problem, in which the reflected spectra were integrated over all viewing angles. The dependence on the viewing angle is especially important in hard X-rays and soft γ-rays, in which regime the reflected spectrum strongly hardens with increasing viewing angle. This is an important effect for modelling γ-ray spectra of active galactic nuclei and Galactic black hole candidates, where the presence of Compton reflection has been established before from X-ray data.

Key words: radiation mechanisms: nonthermal – scattering – galaxies: Seyfert – X-rays: general – gamma-rays: theory.

1 INTRODUCTION

The process of reflection of X-rays and γ-rays from cold matter has become in recent years one of the most important diagnostics of astrophysical Galactic and extragalactic compact sources. The process causes a characteristic hardening in the X-ray spectrum above $\sim$ 10 keV (Lightman & White 1988, hereafter LW88). The hardening is due to the onset of the reflected component, which appears above $\sim$ 10 keV as a result of the increased importance of Compton scattering in comparison with bound-free absorption. The cross-section of the latter, $\sigma_{\rm bf}$, exhibits an overall decrease with increasing energy (except for absorption edges) and becomes less than the Compton cross-section, $\sigma_{\rm C}$, just at energies $\gtrsim$ 10 keV in neutral matter of cosmic composition (Morrison & McCammon 1983). Hence the single-scattering albedo,

$$\lambda(E) \equiv \frac{\sigma_{\rm C}(E)}{\sigma_{\rm C}(E)+\sigma_{\rm bf}(E)}, \tag{1}$$

becomes comparable to unity in that energy range. (Note that both cross-sections have to be defined in the same way, e.g., per hydrogen atom.)

Spectral hardenings characteristic of reflection have been discovered in, among others, Seyfert galaxies by the *Ginga* satellite (Pounds et al. 1990; Nandra & Pounds 1994), and in the Galactic black hole candidate Cyg X-1 (Done et al. 1992; Haardt et al. 1993). We thus infer that in those objects a source of hard X-rays and soft γ-rays is located above some cold medium, e.g., an optically thick accretion disc.

On the other hand, the albedo decreases with energy in soft γ-rays ($\gtrsim$ 50 keV) due to the effect of fast energy loss, preferential forward scattering, and the reduced total scattering cross-section (see LW88). This results in a softening of the total (reflected plus incident) spectrum with respect to the incident component alone. This effect has been found in Seyfert galaxies (Madejski et al. 1995; Zdziarski et al. 1994, 1995).

Green's functions for Compton reflection have been obtained so far only for radiation reflected by a slab and averaged over all viewing angles (White, Lightman & Zdziarski 1988, hereafter WLZ88). LW88 have extended the work of WLZ88 to include bound-free absorption. Some examples of spectra reflected for specific viewing angles have been obtained numerically by Matt, Perola & Piro (1991), George & Fabian (1991), and Hua & Lingenfelter (1992, hereafter HL92). Furthermore, Ghisellini, Haardt & Matt (1994) have obtained the angular dependence of reflected radiation in the non-relativistic limit ($E \lesssim$ 10 keV) in the

© Royal Astronomical Society • Provided by the NASA Astrophysics Data System

1995MNRAS.273..837M

case of $\lambda \lesssim 0.5$ (i.e., when the reflecting medium is not highly ionized). In that case, only the first-order scattering needs to be considered. Then the angle-averaged reflection spectrum can be simply multiplied by a scaling factor dependent on the viewing angle, θ (measured with respect to the slab normal).

However, that simple scaling breaks down at higher energies due to the importance of higher-order scatterings as well as the complex form of the Klein-Nishina differential cross-section. As shown by HL92, the γ-ray part of the reflected spectrum in the case of an incident power-law spectrum strongly hardens with increasing θ. Thus use of the angle-averaged reflection spectra is no longer satisfactory when soft γ-ray spectra of cosmic sources are considered. This is the case, e.g., for Cyg X-1, which contains a reflection component and for which high-quality soft γ-ray spectra have been obtained by the OSSE detector aboard the *Gamma Ray Observatory* (Phlips et al. 1995). By subtracting the properly computed reflection component, one can obtain the spectrum of the intrinsic radiation, which can then reveal the nature of the radiative processes operating in the source. This will become especially important for future high-sensitivity γ-ray observatories like *HEXTE* and *INTEGRAL*.

In this paper, we obtain Green's functions for Compton reflection as a function of the energies of the incident and reflected photons as well as the viewing angle. We perform Monte Carlo calculations, which results are fitted by simple functions. Whenever possible, we employ asymptotic analytic results. We take into account both scattering and absorption.

2 RELATIVISTIC GREEN'S FUNCTIONS FOR COMPTON REFLECTION

We use the Monte Carlo method described by WLZ88 to calculate spectra reflected by a plane-parallel, semi-infinite medium of cold electrons. We first consider the effect of Compton scattering alone, without absorption. The angular distribution of the incident photons is modelled from a distribution uniform in $\mu_i \equiv \cos\theta_i$ (as in WLZ88). Note that this corresponds to $I_{\mu_i} \propto \mu_i^{-1}$. Such irradiation is obtained if the slab is covered by an optically thin source of the primary radiation (in contrast to $I_{\mu_i} =$ constant in the case of an optically thick source of primary radiation above the slab).

The photon Green's function, $G(\mu, x_0, x)$, is calculated on a three-dimensional grid consisting of $\mu \equiv \cos(\theta)$, the energy of incident photons, x_0, and the energy of reflected photons, x. The energies are in units of the electron rest energy, $x \equiv E/m_e c^2$. Green's function is calculated in 10 bins in μ (from 0–0.1 to 0.9–1), and computed for eight values of incident photon energy: $x_0 = 0.01$, 0.0316, 0.1, 0.316, 1, 3.16, 10, and 31.6. For greater incident photon energies the monochromatic albedo decreases below 1 per cent (WLZ88). For $x_0 < 0.01$, Green's function for Compton reflection slowly approaches its non-relativistic limit, with an approximate separation of the dependences on μ and on x. In that case, the angle-dependent factor may be obtained by solving the monochromatic transfer equation (Chandrasekhar 1960). In a Monte Carlo run, we use 10^6 photons followed down to $x = 10^{-4}$, which allow us to confirm that Green's function approaches their asymptotic limit. Conservation of the photon number implies the normalization

$$\int_0^1 \int_0^{x_0} G(\mu, x_0, x)\, \mathrm{d}\mu \mathrm{d}x = 1. \tag{2}$$

In addition, we do runs of 10^7 photons followed over x corresponding to the range of the first four scatterings. This allows us to obtain a better resolution close to x_0, which is particularly important for the first-order scattering, showing a complicated structure in x (see HL92). The distribution of photon energy for scattering order > 4 is nearly Gaussian, which implies a smooth shape of the spectrum far enough from x_0 (cf. Illarionov et al. 1979).

Following WLZ88, our analytic approximations are expressed in terms of the dimensionless wavelength, $y_0 \equiv 1/x_0$, and the wavelength shift, $\Delta y \equiv 1/x - 1/x_0$. The relation $G(\mu, x_0, x) = x^{-2} G(\mu, y_0, \Delta y)$ transforms between the energy and wavelength spaces. In our fits, we first obtain Green's function for $x_0 = 1$ ($e^{\pm}$ pair annihilation emission), and then the ratio, $G(\mu, y_0, \Delta y)/G(\mu, 1, \Delta y)$, for $0.01 < x_0 < 31.6$. To describe the dependence on y_0 and μ, we use coefficients a_i, b_j, c_k in the functional dependence, $G(\mu, y_0, \Delta y) = G\{y_0, \Delta y, a_i[y_0, b_j(\mu, c_k)]\}$.

The results of the Monte Carlo simulations and our fitting functions are shown in Fig. 1. Below, we divide the full range of Δy into two parts. The first, $\Delta y < 2$, is the range of the first-order scattering, in which it dominates. In the second range, $\Delta y > 2$, only higher-order scatterings appear.

2.1 Green's function for $x_0 = 1$

2.1.1 $\Delta y < 2$

In this range, the dominant contribution ($\gtrsim 50$ per cent) is from the first-order scattering. The geometry of the first-order scattering restricts its reflected spectrum to the range of $\Delta y_c < \Delta y < 2$, where $\Delta y_c = 1 - (1 - \mu^2)^{1/2}$. In that range, there is a discontinuity of the first derivative at $\Delta y_d = 1 + (1 - \mu^2)^{1/2}$. In the range of $0 < \Delta y < \Delta y_c$, a weak and neglectable tail from higher-order scatterings appears (see HL92 for detailed discussion). Fig. 2 shows Green's function observed at $\mu = 0.75$ as a function of $\Delta y < 2$.

Note that our Monte Carlo results give spectra integrated over the viewing angle in bins with width $\Delta\mu = 0.1$, and therefore the above discontinuities appear closer to the energy corresponding to the lower boundary of each bin (as shown in Fig. 2). In

Downloaded from https://academic.oup.com/mnras/article/273/3/837/1056423 by guest on 20 August 2022

© Royal Astronomical Society • Provided by the NASA Astrophysics Data System

1995MNRAS.273..837M

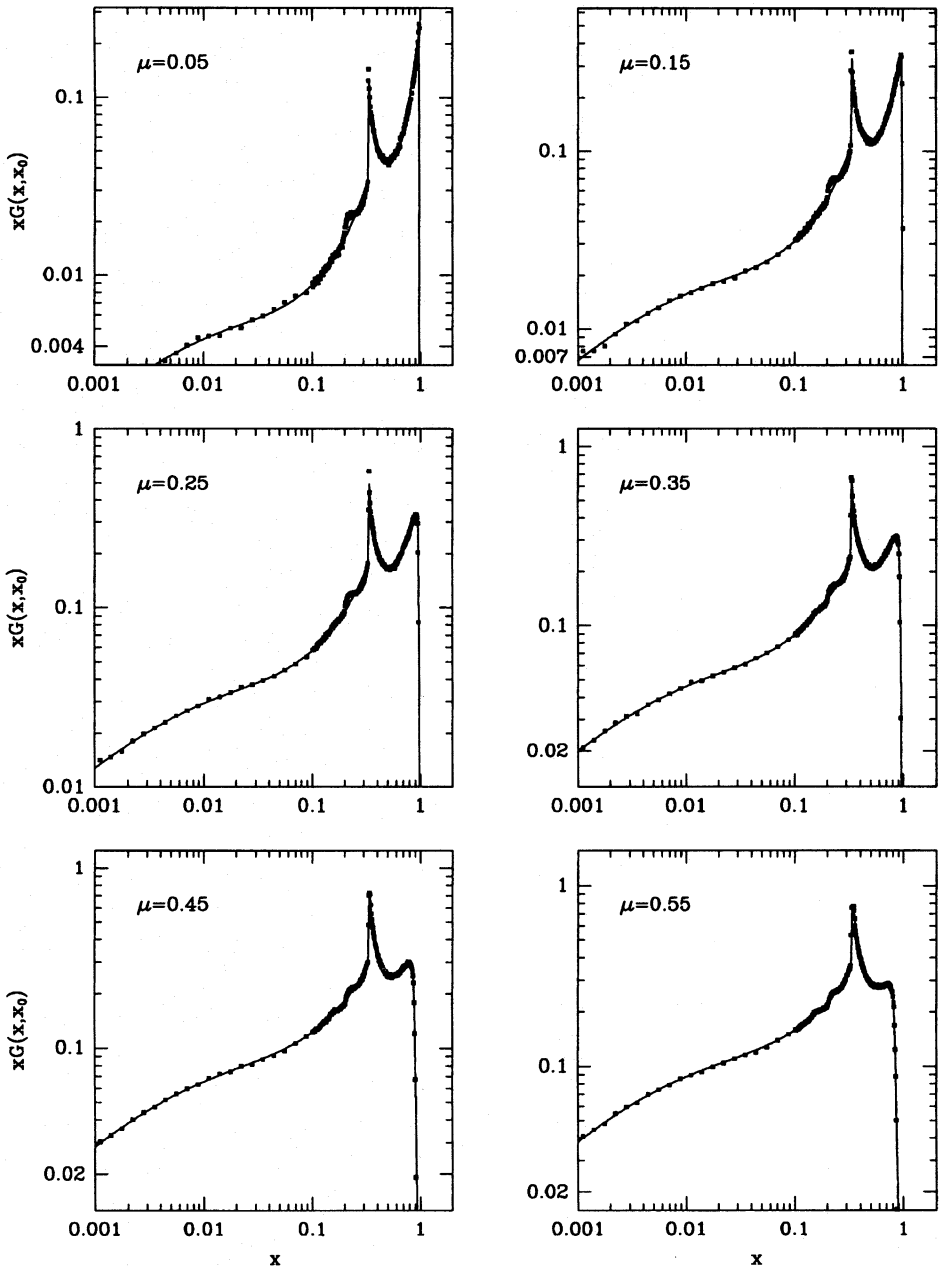

Figure 1. Green's functions for reflection of incident photons of energy $x_0 = 1$ from a plane-parallel, semi-infinite medium. Points indicate the results of Monte Carlo simulations, while solid curves show our fits.

particular, the tail near $\Delta y = 0$ from higher-order scatterings can be cut off at $\Delta y_{cc} = 1 - [1 - (\mu - 0.05)^2]^{1/2}$, above which it is negligible (a cut-off at Δy_c would give the wrong normalization in integrated spectra). The range of validity of our approximations is $\mu = 0.05$–0.95.

In the range $\Delta y_d < \Delta y < 2$, yG is well approximated by a straight line,

$$G(\mu, 1, \Delta y) = \frac{b_0 + b_1(\Delta y - 2)}{1 + \Delta y}, \tag{3}$$

where

$$b_0 = 0.911 - 0.549(1 - \mu)^{1.471}, \qquad b_1 = 0.254 - 0.041\mu^{-3.798}. \tag{4}$$

For $0 < \Delta y < \Delta y_d$, a combination of power laws with an exponential cut-off is used,

$$G(\mu, 1, \Delta y) = \frac{\left\{b_2 + b_3 \max\left[0, (b_4 - \Delta y)\right]^{b_5} + b_6(b_7 - \Delta y)^{b_8}\right\}^{b_9}}{(1 + \Delta y)\left\{1 + \exp\left[b_{10}\left(b_{11} - (\Delta y)^{b_{12}}\right)\right]\right\}}, \tag{5}$$

Downloaded from https://academic.oup.com/mnras/article/273/3/837/1056423 by guest on 20 August 2022

© Royal Astronomical Society • Provided by the NASA Astrophysics Data System

1995MNRAS.273..837M

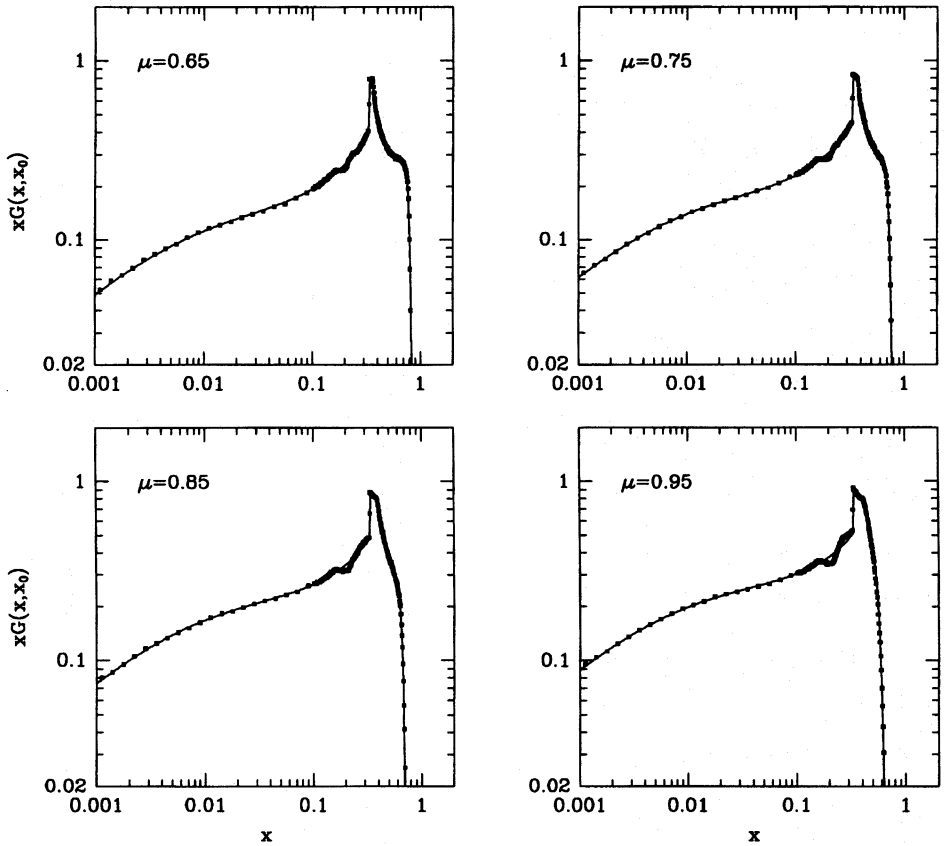

Figure 1 – *continued*

where

$$b_2 = 0.161 + 0.439\mu^{0.189} - 0.791\mu^{7.789}, \qquad b_3 = \max\left[0, \left(-0.871 + 1.740\mu^{0.176} - 1.088\mu^{0.907}\right)\right], \tag{6}$$

$$b_4 = 0.934 + 0.054\mu^{-0.666}, \qquad b_5 = \begin{cases} 4.647 - 11.574\mu + 11.046\mu^2, & \mu < 0.524; \\ 1.615, & \mu > 0.524, \end{cases} \tag{7}$$

$$b_6 = 0.012 + 0.199\mu^{0.939} + 0.861\mu^{8.999}, \qquad b_7 = 2.150, \qquad b_8 = -1.281 + 2.374\mu - 4.332\mu^2 + 2.630\mu^3, \tag{8}$$

$$b_9 = 2.882 + 0.035\mu^{-1.065}, \qquad b_{10} = 30.28 + 69.29\mu, \qquad b_{11} = 1.037\left[1 - (1 - 0.874\mu^2)^{1/2}\right]^{0.123}, \qquad b_{12} = 0.123. \tag{9}$$

Due to the derivative discontinuity of G at Δy_d, we choose to use as the actual approximation to G the minimum of the values obtained from equations (3) and (5).

2.1.2 $\Delta y > 2$

In this range, our approximation to Green's function employs its asymptotic form for $\Delta y \gg 2$, G_{as} [see equation (12) below] as follows:

$$\log\left[\frac{G(\mu, 1, \Delta y)}{G_{as}(\mu, 1, \Delta y)}\right] = \left[b_{14} + b_{15}(\Delta y + 1)^{b_{16}}\right] \log\left(1 + \frac{b_{13}}{\Delta y + 1}\right), \tag{10}$$

where the b_j are given by the polynomial fits,

$$b_j = \sum_{k=0}^{4} c_{jk}\mu^k, \tag{11}$$

and where the coefficients are given in Table 1. A small wave in the reflected spectrum appearing near $\Delta y = 3$ ($x = 0.25$, see Fig. 1) is mainly from the second and third orders of scattering (see Illarionov et al. 1979). Green's function shows a quickly damped wavy shape for $\Delta y > 2$ appearing due to a superposition of subsequent scattering orders. Those waves are not taken into account in our fits, which limits their accuracy in the range $\Delta y = 2$–4 ($x = 0.2$–0.33) to < 12 per cent for $\mu > 0.3$ and to < 20 per cent for $\mu < 0.3$. For Δy either < 2 or > 4, the maximum error does not exceed 5 per cent for $\mu > 0.3$ and 8 per cent for $\mu < 0.3$.

Downloaded from https://academic.oup.com/mnras/article/273/3/837/1056423 by guest on 20 August 2022

© Royal Astronomical Society • Provided by the NASA Astrophysics Data System

1995MNRAS.273..837M

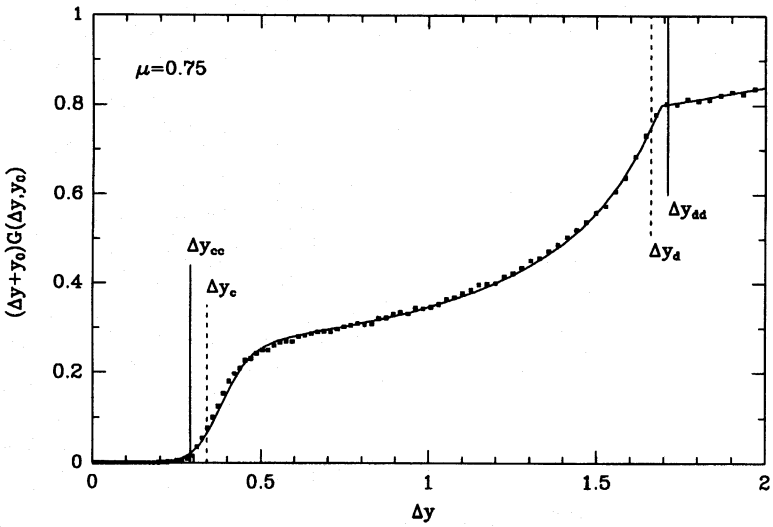

Figure 2. Green's function for $x_0 = 1$ and $\mu = 0.75$. Note that the points from the Monte Carlo simulation are *averaged* over $\mu = 0.70$–0.80. Therefore the discontinuities of the first-order spectrum at Δy_c and Δy_d (defined at the bin centre, $\mu = 0.75$) appear closer to Δy_{cc} and Δy_{dd}, which are defined for the lower boundary of the bin, $\mu = 0.70$.

Table 1. The coefficients c_{jk} (equation 11) for $\Delta y > 2$ and $x_0 = 1$.

$j\backslash k$	0	1	2	3	4
13	56.50	−27.54	671.8	−1245.	708.4
14	−0.897	−0.826	2.273	−0.984	—
15	1.240	−1.297	—	—	—
16	−0.490	1.181	−1.038	—	—

2.1.3 The asymptotic regime of $\Delta y \gg 2$

In this regime, Green's function approaches its non-relativistic form, proportional to $(\Delta y)^{-3/2}$ (see Lightman, Lamb & Rybicki 1981). In that regime, photons have already undergone multiple scatterings, which allows us to separate the angular and energy dependences:

$$G_{\rm as}(\mu, 1, \Delta y) = 1.283 f_{\rm as}(\mu)(\Delta y)^{-3/2}, \tag{12}$$

which is fitted with a double power law and normalized to unity,

$$f_{\rm as}(\mu) = 1.448\left(\mu^{2.033} + 0.745\mu^{1.065}\right). \tag{13}$$

The angular dependence (13) is also valid at any x_0 for $\Delta y \gg 2$, when $G_{\rm as}(\mu, y_0, \Delta y)$ differs from that of equation (12) only in the normalization.

2.2 Green's function for $0.01 < x_0 < 31.6$

Photon wavelength changes in a scattering as $\Delta y = 1 - \cos\vartheta$, where ϑ is the scattering angle, independently of x_0, which is a manifestation of the four-momentum conservation. Thus the overall shape of $G(\Delta y)$ is approximately given by $G[x(\Delta y)]$. This can be seen in Fig. 3, where the spectrum for $x_0 \neq 1$ is roughly the one for $x_0 = 1$ rescaled, especially in the range corresponding to the first order of scattering. In the relativistic regime, the relative energy change per scattering is large because $\Delta y \sim 1$ corresponds to a large energy change. On the other hand, $\Delta x/x \to 0$ in the non-relativistic limit. Hence Green's function for $x_0 \ll 1$ is dominated by a sharp peak near x_0, i.e., the scattering is nearly elastic.

Thus, for $x_0 \lesssim 0.01$, $G(x)$ is sharp enough to treat the effective dependence on μ by averaging over x (with most of the contribution from $\Delta x \lesssim 4x_0^2$). Hence the angle-dependent Green's function can be replaced by the angle-averaged Green's function multiplied by an angle-dependent coefficient (normalized to unity),

$$G(\mu, y_0, \Delta y) \approx G_{\rm av}(\Delta y, y_0) f(\mu), \tag{14}$$

Downloaded from https://academic.oup.com/mnras/article/273/3/837/1056423 by guest on 20 August 2022

© Royal Astronomical Society • Provided by the NASA Astrophysics Data System

1995MNRAS.273..837M

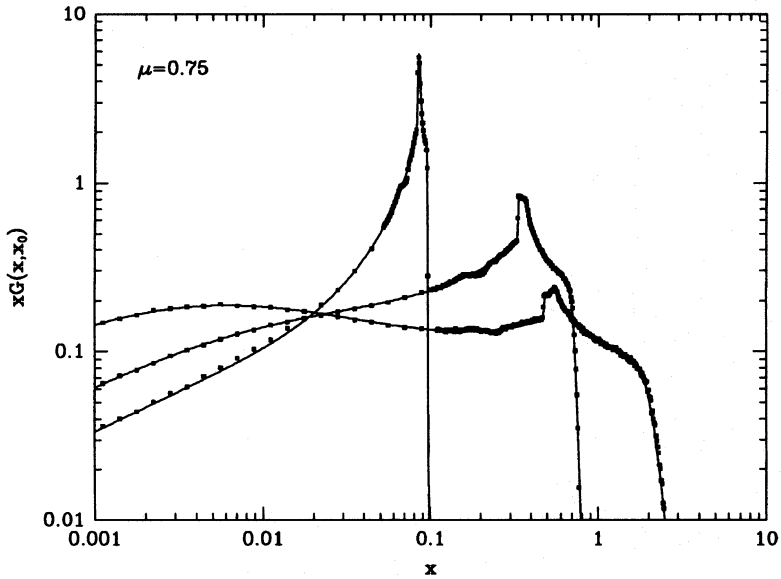

Figure 3. Green's functions for $x_0 = 0.1$, 1, 10 at $\mu = 0.75$. The points give the results of Monte Carlo simulations, whereas the solid curves give the fits.

where

$$f(\mu) = 1.844\mu^{0.844}. \tag{15}$$

This gives an accuracy $\lesssim 2$ per cent in the range $x_0 < 0.01$ for spectra with a local power-law slope, $\alpha > 0$; for $\alpha < 0$, the error increases with decreasing α. The angle-averaged Green's function is given by WLZ88 at any x_0. Note that it achieves its Thomson-limit form (Lightman et al. 1981) rather slowly, only for $x_0 \lesssim 10^{-4}$. Note the difference between equations (13) and (15). The former gives the angular dependence of Green's function in the limit $\Delta y \gg 2$ for any x_0. The latter gives the angular dependence of Green's function for $x_0 \lesssim 0.01$ and for broad incident spectra with $\alpha \gtrsim 0$ only. The reflected spectrum can then be obtained by integrating equation (14) over the incident spectrum, with most of the contribution to the integral from $\Delta y \lesssim 4$. Instead of the integration, one can also use a δ-function approximation to Green's function (see Section 3.2 below).

2.2.1 $\Delta y < 2$

The spectrum from the first-order scattering expressed as a function of Δy is relatively weakly dependent on x_0. In particular, the characteristic wavelength shifts, Δy_c and Δy_d, do not depend on x_0 (see Section 2.1.1). Since the first-order scattering dominates in the range of $\Delta y < 2$, we expect that $G(\Delta y)$ will be relatively weakly dependent on x_0.

Thus we normalize Green's function for $\Delta y < 2$ to that for $x_0 = 1$ (see Section 2.1.1), and fit the ratio using a third-order polynomial. For $0.1 < x_0 < 31.6$, we obtain

$$\log\left(\frac{G(\mu, y_0, \Delta y)}{G(\mu, 1, \Delta y)}\right) = \log\left(\frac{\Delta y + 1}{\Delta y + y_0}\right) + \sum_{i=0}^{3} a_i \left[\frac{\log\left(\frac{2+y_0}{\Delta y + y_0}\right)}{\log\left(\frac{2+y_0}{y_0}\right)}\right]^i, \tag{16}$$

where

$$a_i = \log y_0 \sum_{j=0}^{4} b_{ij} \log^j y_0, \qquad b_{ij} = \sum_{k=0}^{4} c_{ijk}\mu^k + c_{ij5} \exp\left[c_{ij6}(\mu - c_{ij7})\right]. \tag{17}$$

The coefficients c_{ijk} are given in Table 2. This approximation fails in the tail of $\Delta y < \Delta y_{cc}$, where the (negligible) spectrum should be set to zero.

For $0.01 < x_0 < 0.1$, the function $G(\mu, y_0 = 10, \Delta y)$ can be simply scaled because the range of $0 < \Delta y < 2$ becomes a very narrow interval of x ($\Delta x \simeq 2x_0^2$),

$$\frac{G(\mu, y_0, \Delta y)}{G(\mu, 10, \Delta y)} = a_4, \tag{18}$$

Downloaded from https://academic.oup.com/mnras/article/273/3/837/1056423 by guest on 20 August 2022

© Royal Astronomical Society • Provided by the NASA Astrophysics Data System

1995MNRAS.273..837M

Table 2. The coefficients c_{ijk} (equation 17) of the approximation to G for $\Delta y < 2$ and $0.1 < x_0 < 31.6$.

$i=0$								
$j\backslash k$	0	1	2	3				
0	0.8827	−0.5885	0.7988	−0.4117				
1	0.0517	0.1076	−0.1691	0.0678				
2	0.0014	0.0043	—	—				
3	−0.0003	−0.0027	0.0021	—				
$i=1$								
$j\backslash k$	0	1	2	3	4	5	6	7
0	−1.3259	1.6214	−3.7007	2.1722	—	1	20.3	1.063
1	0.0790	−0.4029	0.6619	0.2210	—	−1	17.7	1.041
2	0.0751	−0.1848	0.4068	−0.4126	—	1	9.8	1.185
3	−0.0020	−0.0394	0.1004	−0.0597	—	—	—	—
$i=2$								
$j\backslash k$	0	1	2	3	4	5	6	7
0	3.2953	−3.6996	7.9837	−4.6855	—	—	—	—
1	−0.5278	0.9857	−1.7454	−0.3464	—	1	27.6	0.959
2	−0.1919	0.5798	−1.2879	1.4885	—	−1	18.3	0.986
3	0.0200	0.0832	−0.0333	−0.2370	—	1	16.6	1.086
$i=3$								
$j\backslash k$	0	1	2	3	4	5	6	7
0	−2.2779	2.4031	−4.0733	1.9499	—	−1	19.6	0.968
1	0.4790	−1.0166	3.1727	−4.0108	3.0545	−1	30.4	0.957
2	0.1122	−0.3580	0.4985	−0.3750	−0.5349	1	31.2	0.972
3	−0.0160	−0.0471	−0.0536	0.2006	0.2929	−1	30.6	1.009
4	0.0005	0.0021	−0.0447	0.1749	−0.2303	1	16.9	1.130

where

$$a_4 = 1 + b_0 \left\{ 0.326 \left[\left(\frac{y_0}{10} \right)^{1.692} - 1 \right] + \log \left(\frac{y_0}{10} \right) \right\}, \qquad b_0 = 0.006 + 0.089\mu - 0.102\mu^2 + 0.056\mu^3. \tag{19}$$

2.2.2 $\Delta y > 2$

In the range $\Delta y > 2$ and $0.01 < x_0 < 31.6$, we have found a fit,

$$\log \left[\frac{G(\mu, y_0, \Delta y)}{G(\mu, 1, \Delta y)} \right] = \log \left(\frac{\Delta y + 1}{\Delta y + y_0} \right) + \log a_5 + a_7 \left(1 + \frac{a_8}{\Delta y + y_0} \right) \log \left(1 + \frac{a_6}{\Delta y + y_0} \right), \tag{20}$$

where

$$a_5 = 0.763 y_0^{-0.507} + 0.007 y_0^{-1.553} + 0.033 \log y_0 + 0.230, \qquad a_6 = 75.180 y_0^{-1}, \tag{21}$$

$$a_7 = 0.100 y_0^{1.623} + 0.115 \log y_0 - 0.100, \qquad a_8 = \begin{cases} b_1 + b_2 \log y_0, & y_0 < 1; \\ b_3 + b_4 \log y_0 + b_5 \left(b_6 + y_0^{-1} \right)^{b_7}, & y_0 > 1, \end{cases} \tag{22}$$

and

$$b_j = \sum_{k=0}^{3} c_{jk} \mu^k, \tag{23}$$

with the coefficients given in Table 3. In the limit of $\Delta y \gg 2$, $G(y_0)$ differs from $G(y_0 = 1)$ only in the normalization, a_5 (see Section 2.1.3).

For $x_0 > 1$ and any Δy, the maximum error is < 10 per cent for $\mu > 0.3$ and < 20 per cent for $\mu < 0.3$. For $x_0 < 1$ and Δy either < 2 or > 4, the maximum error is < 5 per cent for $\mu > 0.3$ and < 12 per cent for $\mu < 0.3$. The error in the range of $2 < \Delta y < 4$ (and $x_0 < 1$) is < 30 per cent, and it is largest for the lowest value of $x_0 = 0.01$. This is because Green's function is increasingly peaked at $\Delta y = 2$; also, the wave near $\Delta y = 3$ is becoming stronger with decreasing x_0 (see Fig. 3). On the other hand, Δx per scattering decreases with decreasing x_0, which makes the energy span corresponding to $2 < \Delta y < 4$ narrower. Thus the error for a broad incident spectrum can even decrease for small x.

Downloaded from https://academic.oup.com/mnras/article/273/3/837/1056423 by guest on 20 August 2022

© Royal Astronomical Society • Provided by the NASA Astrophysics Data System

1995MNRAS.273..837M

Table 3. The coefficients c_{jk} (equation 23) for $\Delta y > 2$ and $0.01 < x_0 < 31.6$.

$j\backslash k$	0	1	2	3
1	0.618	−0.830	—	—
2	0.128	−0.132	—	—
3	0.632	−0.875	—	—
4	−0.672	−0.286	0.717	−0.481
5	0.0126	−0.0160	0.0077	—
6	0.0111	0.0030	−0.0014	—
7	−2.437	−0.328	−0.260	0.279

3 COMPTON SCATTERING AND ABSORPTION

3.1 Impact of absorption on Green's function

Green's function can be decomposed into contributions from each order of scattering,

$$G(\mu, y_0, \Delta y) = \sum_{i=1}^{\infty} g_i(\mu, y_0, \Delta y). \tag{24}$$

In cosmic-composition matter, bound-free absorption is negligible above $\sim$ 30 keV (e.g., Morrison & McCammon 1983). Thus absorption can be important only in the non-relativistic regime of scattering. Furthermore, absorption is unimportant for initial photons with $x_0 \gtrsim 1$, which have to lose most of their energy by scattering before entering the energy range in which absorption is important. Therefore we need to develop a formalism for absorption of photons with $x_0 \ll 1$ only. This formalism can then be applied at any x_0 with negligible errors.

For photons with $x_0 \ll 1$, the relative energy loss per scattering is small, and the distribution of photons that have undergone a given number, $(i-1)$, of scatterings is narrow. Then the average single-scattering albedo for those photons,

$$\bar{\lambda}_i(y_0) = \frac{\int_0^\infty \lambda(y_0+\Delta y)\tilde{g}_{i-1}(y_0,\Delta y)\,\mathrm{d}(\Delta y)}{\int_0^\infty \tilde{g}_{i-1}(y_0,\Delta y)\,\mathrm{d}(\Delta y)}, \tag{25}$$

is representative for most of them, and the ith order of scattering is suppressed by $\bar{\lambda}_i(y_0)$. Here, $\tilde{g}_i$ is the distribution of photons that have not escaped after the ith scattering. Then Green's function in the presence of absorption may be written as

$$G_{\rm abs}(\mu, y_0, \Delta y) = \sum_{i=1}^{\infty} g_i(\mu, y_0, \Delta y) \prod_{k=1}^{i} \bar{\lambda}_k(y_0). \tag{26}$$

The average wavelength shift for the ith order of scattering is $\Delta y \lesssim i$ for $x_0 \lesssim 1$ (in the Thomson limit, $\Delta y = i$ exactly, see Illarionov et al. 1979). Thus the dominant contribution to Green's function at $\Delta y = i$ is from the ith order of scattering. The average albedo at this wavelength can then be approximated by $\bar{\lambda}_i(y_0) \approx \lambda(y_0 + i - 1)$, which allows a separation of the effects of absorption and scattering. We find numerically that the best overall approximation is $\bar{\lambda}_i(y_0) \approx \lambda(y_0 + \Delta y - 0.15)$ [used in an integration limit in equation (27) below]. The range $\Delta y < 2$ needs to be considered separately because the photon distribution after the first scattering is distinctly different from that for higher-order scattering (see Illarionov et al. 1979); also, relative contributions from the first and higher-order scattering depend on λ. We can thus write

$$G_{\rm abs}(\mu, y_0, \Delta y) \approx G(\mu, y_0, \Delta y) \begin{cases} \lambda(y_0)\left\{a(\mu) + [1-a(\mu)]\left[1 + h(\Delta y)(1-\lambda)^{1/2}\right] \exp\left[\int_0^{\Delta y} \mathrm{d}k \ln \lambda(y_0+k)\right]\right\}, & \Delta y < 2; \\ \exp\left[\int_0^{\Delta y - 0.15} \mathrm{d}k \ln \lambda(y_0+k)\right], & \Delta y > 2, \end{cases} \tag{27}$$

where

$$a(\mu) = 0.802 - 1.019\mu + 2.528\mu^2 - 3.198\mu^3 + 1.457\mu^4 + 8.10 \times 10^{-7}\mu^{-4}, \tag{28}$$

$$h(\Delta y) = \exp(0.381\Delta y) - 2 \tag{29}$$

are the factors describing the dependence of the albedo for the first order of scattering with respect to the total reflection for $\Delta y < 2$ on μ and Δy, respectively. [Note that $\lambda(y_0+k)$ in equation (27) denotes λ at y_0+k.] In the case of $\sigma_{\rm bf}/\sigma_{\rm T} = Cx^{-3}$ which is approximately valid when $E \gtrsim 10$ keV, the integral in equation (27) may be calculated analytically:

$$\int \mathrm{d}k \ln \lambda(y_0+k) = (y_0+k)\left\{3 - \ln\left[1 + C(y_0+k)^3\right]\right\} + \frac{1}{2C^{1/3}} \ln\left\{\frac{1 - C^{1/3}(y_0+k) + C^{2/3}(y_0+k)^2}{\left[1 + C^{1/3}(y_0+k)\right]^2}\right\} - \frac{\sqrt{3}}{C^{1/3}} \arctan\left\{\frac{1}{\sqrt{3}}\left[2C^{1/3}(y_0+k) - 1\right]\right\}. \tag{30}$$

Downloaded from https://academic.oup.com/mnras/article/273/3/837/1056423 by guest on 20 August 2022

© Royal Astronomical Society • Provided by the NASA Astrophysics Data System

1995MNRAS.273..837M

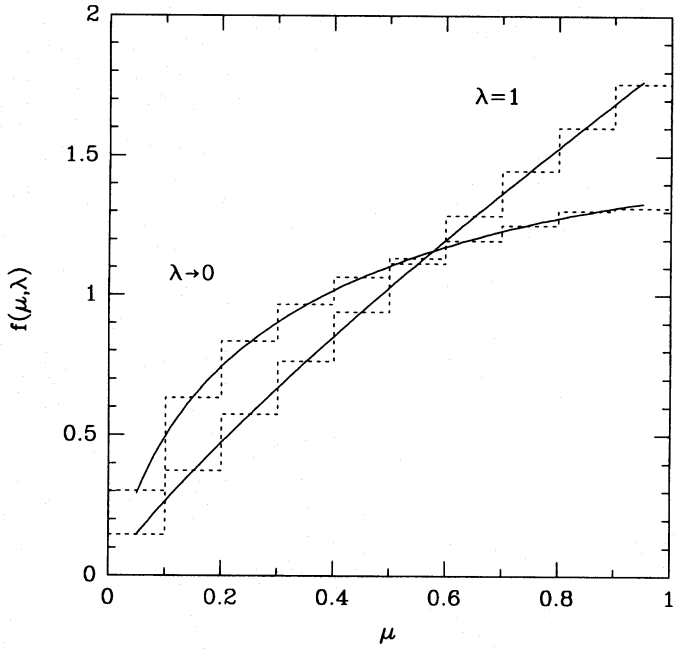

Figure 4. The normalized angular dependence of Green's function in the non-relativistic limit in the cases of dominant absorption ($\lambda \to 0$) and no absorption ($\lambda = 1$). Solid curves give the analytical solutions, and the dashed histograms give the results of Monte Carlo simulations.

The error of equations (27)–(30) is < 5 per cent for spectra with $\alpha > 0$ at any x_0 and λ. The error may become large for $\alpha < 0$ because of a contribution from the range 30 keV < E < 60 keV, where both the first-order scattering distribution is broad and absorption is not yet completely negligible, which causes the approximation based on the averaged factors $a(\mu)$ and $h(\Delta y)$ to fail. We note that the analogous method of LW88 for including the effect of absorption on the angle-averaged Green's function for $\lambda \gtrsim 0.5$ breaks down for the angle-dependent Green's function. This is mostly because the function suppressing scattering due to absorption was calculated in the non-relativistic limit, whereas the reflected spectrum for different viewing angles contains different fractions of photons from higher-order scatterings, for which x_0 is in the relativistic regime.

3.2 The non-relativistic limit

Absorption reduces strongly the contribution of higher-order scatterings to the reflected spectrum [see equation (26)]. For strong enough absorption, the first-order scattering dominates, with its contribution reduced by the albedo, $\lambda(y_0)$. Also, the energy change per scattering is small in the non-relativistic limit, $x_0 - x \lesssim 2x_0^2$ (see Section 2.2), i.e., Compton scattering is nearly elastic.

We can then treat Compton reflection as diffuse monochromatic radiation transfer with the Rayleigh phase function, $(3/4)(1+\cos^2\vartheta)$, and replace Green's function with $G(\mu, x, x_0) \approx F(\mu,\lambda)\delta(x - x_0)$, where $F(\mu,\lambda)$ is the solution of the transfer equation. The general solution of this problem in terms of the H-functions was presented by Chandrasekhar (1960). After the first scattering the photon distribution is nearly isotropic and the isotropic phase function can be used. Accordingly, we divide the flux $F(\mu,\lambda)$ into two parts:

$$F(\mu,\lambda) = F^1(\mu,\lambda) + F^{>1}(\mu,\lambda), \tag{31}$$

where

$$F^1(\mu,\lambda) = \frac{3\lambda}{16}\mu\left[\left(3 - 2\mu^2 + 3\mu^4\right)\ln\left(1+\frac{1}{\mu}\right) + \left(3\mu^2 - 1\right)\left(\frac{1}{2} - \mu\right)\right] \tag{32}$$

describes the first-order reflection [Ghisellini et al. (1994); note that their equation gives the normalized flux, equation (34) below, in the limit $\lambda \ll 1$]. For higher orders we obtain

$$F^{>1}(\mu,\lambda) = \frac{\lambda\mu}{2}\ln\left(1+\frac{1}{\mu}\right)\left\{\left[1+\left(\frac{1}{\sqrt{1-\lambda}}-1\right)\left(1-\frac{\ln\left(1+\sqrt{3(1-\lambda)}\right)}{\sqrt{3(1-\lambda)}}\right)\right]\frac{1+\mu\sqrt{3}}{1+\mu\sqrt{3(1-\lambda)}}-1\right\}, \tag{33}$$

using the approximation of H-functions for radiation transfer with the isotropic phase function given by Basko (1978). In the limit of $\lambda \to 1$, the factor in curly brackets becomes $\approx (1+\sqrt{3}/2)(1+\mu\sqrt{3})[1-(1+\mu\sqrt{3})(1-\lambda)^{1/2}+...]-1$. If $\lambda(E) < 0.5$, higher-order scatterings are strongly suppressed and the contribution of $F^{>1}$ is negligible. Equation (32) then gives the accuracy < 2 per cent

Downloaded from https://academic.oup.com/mnras/article/273/3/837/1056423 by guest on 20 August 2022

© Royal Astronomical Society • Provided by the NASA Astrophysics Data System

1995MNRAS.273..837M

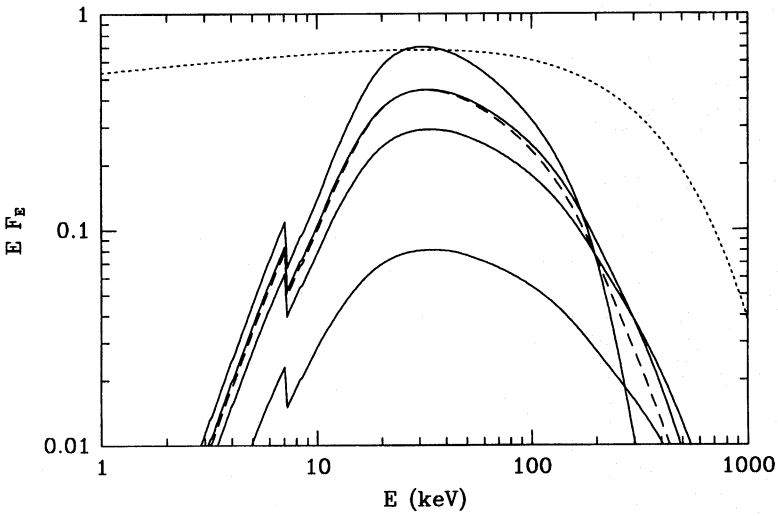

Figure 5. The reflected spectra (solid curves) from a power-law spectrum with an exponential cut-off (dotted curve) incident on a plane-parallel, semi-infinite medium. The energy spectral index of the incident spectrum is $\alpha = 0.9$ and the cut-off energy is $E_c = 300$ keV. The viewing angles correspond to $\mu = 0.05, 0.25, 0.45, 0.95$, from bottom to top, respectively. The dashed curve gives the angle-averaged reflection spectrum.

for $E \leqslant 25$ keV. The contribution of $F^{>1}$ grows with increasing λ, and the error of equations (32)–(33) is < 6 per cent for $E \leqslant 12$ keV and $0.5 < \lambda < 0.77$, and < 12 per cent for $0.77 < \lambda < 0.9$.

When $\lambda \simeq 1$ (i.e., vanishing absorption), equations (32)–(33) fail because then an appreciable number of incident photons get downscattered to the lower energies. This causes an excess of photons in the reflected spectrum below ~ 10 keV with respect to the predictions of equations (32)–(33), in particular for hard spectra with $\alpha \lesssim 1$.

In the case of nearly full ionization ($\lambda > 0.9$), we can instead use the average Green's function of WLZ88 and treat absorption using the method described in Section 3.1. The angular dependence is then given by the normalized flux,

$$f(\mu, \lambda) = \frac{F(\mu, \lambda)}{\overline{F}(\lambda)}, \tag{34}$$

where

$$\overline{F}(\lambda) = \frac{1 - \sqrt{1-\lambda}}{1 + \sqrt{1-\lambda}} \tag{35}$$

is the angle-averaged monochromatic flux obtained by solving the transfer equation exactly. In the limiting case of $\lambda = 1$, the angular factor is described by equation (15), which yields accuracy < 10 per cent for $\lambda > 0.99$ and $\alpha > 0$. For $\alpha \lesssim 0$, the accuracy worsens because the tail of Green's function from higher-order scattering becomes important. Generally, the elastic approximation works well with relatively slowly varying incident spectra (the local $|\alpha| < 2$) only, because in this case deviations of Green's function from a δ-function are effectively averaged. Fig. 4 shows the factor (34) in the limits of dominant and vanishing absorption.

4 DISCUSSION AND APPLICATIONS

In order to facilitate the use of our results, Table 4 gives a short guide for calculating Green's function. The reflected spectrum for any incident spectrum can then be obtained by the following integration (obtained from the definition of Green's function):

$$S_{\rm ref}(x) = \int_0^{\frac{1}{x}} S_{\rm inc}\left(\frac{x}{1 - x\Delta y}\right) G\left(\mu, \frac{1 - x\Delta y}{x}, \Delta y\right) \frac{{\rm d}(\Delta y)}{1 - x\Delta y}. \tag{36}$$

In the numerical integration one has to treat the peak of Green's function at $\Delta y = 2$ with care. This peak is much more pronounced in the x-space, which is the reason for using Δy as the integration variable.

Our approximations to Green's function are then used to calculate the reflected spectra for an incident power-law spectrum with an exponential cut-off with the parameters typical for Seyfert 1s (Madejski et al. 1995; Zdziarski et al. 1995), shown in Fig. 5. We assume absorption in neutral [except for ionized H and He, as expected in accretion discs (Ross & Fabian 1993)], solar-composition matter, as given by Bałucińska-Church & McCammon (1992) below 10 keV and extrapolated with $\sigma_{\rm bf} \propto E^{-3}$ above 10 keV. The error of the approximation to the reflected spectra is < 5 per cent in the 20–60 keV range (where our fits slightly overestimate the corresponding Monte Carlo spectra), and $\lesssim 1$ per cent at other energies.

Downloaded from https://academic.oup.com/mnras/article/273/3/837/1056423 by guest on 20 August 2022

© Royal Astronomical Society • Provided by the NASA Astrophysics Data System

1995MNRAS.273..837M

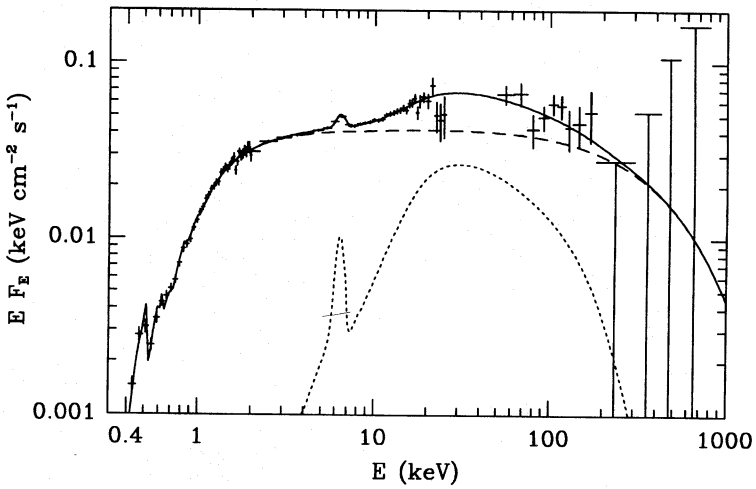

Figure 6. A broad-band spectrum (crosses) of IC 4329A from *ROSAT*, *Ginga*, and OSSE (Madejski et al. 1995). The dashed curve gives the absorbed incident spectrum, the dotted curve gives the reflected component including a fluorescent Fe Kα line, and the solid curve is the sum. See text for the spectral parameters. The equivalent width of the line is 120 eV. Absorption is due to both neutral ($n_H = 2.1 \times 10^{21}$ cm^{-2}) and ionized media ($n_H = 3.3 \times 10^{21}$ cm^{-2} with the ionization parameter of $\xi = 1.6$, using the formalism described in Zdziarski et al. 1995).

Table 4. The numbers of the main equations for the approximations to Green's function at different ranges of energy and albedo.

	$E_0 < 12$ keV
$\lambda < 0.5$	(32)
$0.5 < \lambda < 0.9$	(31-33)
$\lambda > 0.9$	(31-35)+WLZ88
$\lambda > 0.99$	(15)+WLZ88

	12 keV$< E_0 <$ 51 keV	$E_0 > 51$ keV
$x < \frac{x_0}{1+2x_0}$	(10),(12),(20),(27)	
$x > \frac{x_0}{1+2x_0}$	min[(3),(5)],(16),(18),(27)	min[(3),(5)],(16),(27)

The reflected spectrum for $\mu = 0.45$ is closest in overall shape to the reflected spectrum averaged over all viewing angles (Fig. 5). We note that the actual reflected angle-averaged spectrum is higher by up to 6 per cent in the 11–20 keV range than that obtained using the method of LW88. The difference is mostly due to the approximate treatment of absorption in LW88.

Also, the shape of the reflected spectrum in Fig. 5 at any angle is the same as that of the angle-averaged spectrum at $E \leqslant 10$ keV. The scaling of equation (32) can then be used (Ghisellini et al. 1994). On the other hand, the two spectra can be very different above 10 keV. In particular, the face-on reflected spectrum becomes significantly harder than the angle-averaged one. The ratio of the spectra is 1.33 below 10 keV and 1.59 at 30 keV. One should bear this in mind when applying Green's functions of LW88 to X-ray spectra of Seyfert 1s, which are expected to be oriented close to face-on (Antonucci 1993).

We illustrate the use of our angle-dependent Green's functions on the spectrum of IC 4329A, a bright Seyfert 1. Fig. 6 shows its spectrum with the same data sets as in model D of Madejski et al. (1995). They fitted the data using the angle-averaged reflection and obtained a relative normalization of reflection $R = 1.04^{+0.26}_{-0.23}$, $\alpha = 0.93^{+0.03}_{-0.03}$, and an exponential cut-off energy $E_c = 320^{+150}_{-80}$ keV (all errors here are for 90 per cent confidence for one interesting parameter, i.e., $\Delta\chi^2 = 2.7$). We have assumed the viewing angle to be close to face-on, $\theta = 30°$, which yields $R = 0.68^{+0.16}_{-0.14}$, $\alpha = 0.96^{+0.03}_{-0.03}$, and $E_c = 410^{+270}_{-120}$ keV. If one used instead equation (32) to rescale the angle-averaged spectrum to that at 30° (Ghisellini et al. 1994), one would get $R \approx 0.80^{+0.20}_{-0.18}$ as the best-fitting value, i.e., somewhat more than in the presented fits. The above fit has been obtained using the XSPEC spectral fitting package (Shafer, Haberl & Arnaud 1991), into which we incorporated a model with our approximations.

We have also re-fitted the average spectrum of weaker Seyfert 1s observed by both *Ginga* and OSSE (Zdziarski et al. 1995). Zdziarski et al. (1995) obtained $R = 1.3^{+0.3}_{-0.2}$, $\alpha = 0.92^{+0.03}_{-0.03}$ and $E_c = 560^{+840}_{-240}$ keV using the angle-averaged reflection. On the other hand, we obtain $R = 0.66^{+0.13}_{-0.12}$, $\alpha = 0.88^{+0.04}_{-0.05}$, and $E_c = 430^{+300}_{-170}$ keV for the fixed inclination angle of 30°. The amplitude of the fluorescent Fe Kα line is treated as a free parameter. We see that now there is substantially less reflection than $R \approx 1.0^{+0.2}_{-0.2}$ expected from simple rescaling of the angle-averaged spectrum. Our value is in close agreement with both the result for IC 4329A above and the average reflection fraction in Seyferts obtained by Nandra & Pounds (1994). Thus either the cold matter seen from the power-law source covers only a $\sim 1.3\pi$ solid angle, or a part of our view of the cold matter is blocked.

We have compared our reflected spectra with the Monte Carlo model CD_D2A incorporated into XSPEC by Ian George. The model uses results of George & Fabian (1991; note that they used the non-relativistic form of the differential scattering cross-section) for power-law incident spectra with a sharp cut-off at 70 keV. For $\alpha = 0.9$ we obtain a good general agreement up to ~ 20 keV. At 28 keV (which appears to be the highest usable energy of the model CD_D2A), our Monte Carlo spectrum is higher by 5 per cent than that of George.

Downloaded from https://academic.oup.com/mnras/article/273/3/837/1056423 by guest on 20 August 2022

© Royal Astronomical Society • Provided by the NASA Astrophysics Data System

1995MNRAS.273..837M

5 SUMMARY

We have fitted the angle-dependent Green's functions for Compton reflection by simple, closed-form functions. We assumed a plane-parallel, semi-infinite medium irradiated by photons with the angular distribution corresponding to emission of an optically thin corona above the slab. The approximations have been obtained both in the relativistic regime, where the energy loss due to Compton scattering is significant and the reflected spectrum has to be calculated by integrating Green's function, and in the non-relativistic limit, where Compton scattering may by treated as nearly elastic and an appropriate transfer equation can be used. We have also taken into account the effect of absorption (mostly bound-free) on the reflected spectra. Our results on the effect of absorption are especially important in the mildly relativistic range, 10 keV $\lesssim E \lesssim$ 60 keV. We find that there are significant differences between the angle-dependent reflection spectra and the averaged ones. In particular, the face-on reflected spectrum in the case of the $\alpha = 1$ incident power law is both significantly harder in the $\sim$ 10–30 keV range and softer above 30 keV than the angle-averaged spectrum. FORTRAN codes incorporating our approximations (in particular codes in the XSPEC format) can be obtained from the authors via e-mail.

ACKNOWLEDGMENTS

This research has been supported in part by the NASA grants NAG5-2439, NAGW-3129, and NAG5-1813, and the Polish KBN grant 221129102.

REFERENCES

Antonucci R. R. J., 1993, ARA&A, 31, 473
Bałucińska-Church M., McCammon D., 1992, ApJ, 400, 699
Basko M. M., 1978, ApJ, 223, 268
Chandrasekhar S., 1960, Radiative Transfer. Dover Publications, Inc., New York
Done C., Mulchaey J. S., Mushotzky R. F., Arnaud K. A., 1992, ApJ, 395, 275
George I. M., Fabian A. C., 1991, MNRAS, 249, 352
Ghisellini G., Haardt F., Matt G., 1994, MNRAS, 267, 743
Haardt F., Done C., Matt G., Fabian A. C., 1993, ApJ, 411, L95
Hua X.-M., Lingenfelter R. E., 1992, ApJ, 397, 591 (HL92)
Illarionov A., Kallman T., McCray R., Ross R., 1979, ApJ, 228, 279
Lightman A. P., White T. R., 1988, ApJ, 335, 57 (LW88)
Lightman A. P., Lamb D. Q., Rybicki G. B., 1981, ApJ, 248, 738
Madejski G. M. et al., 1995, ApJ, 438, 672
Matt G., Perola G. C., Piro L., 1991, A&A, 247, 25
Morrison R., McCammon D., 1983, ApJ, 270, 119
Nandra K., Pounds K., 1994, MNRAS, 268, 405
Phlips B. F. et al., 1995, ApJ, submitted
Pounds K. A., Nandra K., Stewart G. C., George I. M., Fabian A. C., 1990, Nat, 344, 132
Ross R. R., Fabian A. C., 1993, MNRAS, 261, 74
Shafer R. A., Haberl F., Arnaud K. A., 1991, XSPEC: An X-ray Spectral Fitting Package. ESA TM-09, ESA, Paris
White T. R., Lightman A. P., Zdziarski A. A., 1988, ApJ, 331, 939 (WLZ88)
Zdziarski A. A., Fabian A. C., Nandra K., Celotti A., Rees M. J., Done C., Coppi P. S., Madejski G. M., 1994, MNRAS, 269, L55
Zdziarski A. A., Johnson N. W., Done C., Smith D., McNaron-Brown K., 1995, ApJ, 438, L63

This paper has been produced using the Royal Astronomical Society/Blackwell Science LaTeX style file.

Downloaded from https://academic.oup.com/mnras/article/273/3/837/1056423 by guest on 20 August 2022

© Royal Astronomical Society • Provided by the NASA Astrophysics Data System